Soils and Foundations 2015;55(4):829–840

The Japanese Geotechnical Society

Soils and Foundations

www.sciencedirect.com
journal homepage: www.elsevier.com/locate/sandf

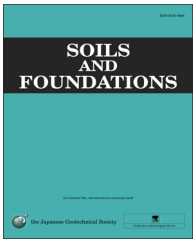

Influence of location of subsurface structures on development of underground cavities induced by internal erosion

Mari Sato*, Reiko Kuwano

School of Agriculture, Kyoto University Oiwake-cho, Kitashirakawa, Sakyo-ku, Kyoto 606-8502, Japan
Institute of Industrial Science, the University of Tokyo, Bw304, 4-6-1, Komaba, Meguro-ku, Tokyo 153-8505, Japan

Received 7 November 2014; received in revised form 18 March 2015; accepted 17 April 2015
Available online 21 July 2015

Abstract

This paper revealed the influence of buried structures on the development of underground cavities with internal erosion from the breakage of sewer pipes, and investigated the spatial distribution of a loose ground where the strength was decreased due to this erosion. Moreover, the collapse of the underground cavities induced sinkhole accidents. A series of laboratory model tests was conducted to examine the relevance of the locations of subsurface structures and the expansion of underground cavities. Following the model tests, the strength of the model ground was examined by means of a series of laboratory penetration tests. The results of these laboratory tests showed that the subsurface structures brought about a variation in the formation of cavities as a result of a variation in the pathway of localized seepage that had developed throughout the nearest path from the surface to the cracks in the pipes. In addition, this paper found that developments in the loose ground were induced without the accompaniment of visible deformation. A large-scale model test indicated the applicability of the results of the laboratory model tests to the practical scale of the ground. Overall, we proposed the necessity of considering the mutual effect of subsurface structures on the progression of cavity expansion due to internal erosion.

Keywords: Sinkhole; Sewer pipes; Internal erosion; Model test; Penetration resistance

1. Introduction

Sinkhole accidents along urban traffic ways are induced by the failure of underground cavities that have mainly developed due to internal erosion (Bonelli, 2012) from the breakage of sewer pipes (e.g., Tohda and Yoshimura, 2001; Tohda and Hachiya, 2005). Fig. 1 illustrates the process, namely, an underground cavity developed due to the discharge of soil to the cracks accompanying internal erosion with a seepage flow. Sinkholes induced by the growth of a cavity can sometimes endanger lives and property; therefore, measures have recently been taken to prevent such accidents. One of the main measures is the detection of underground cavities using GPR (ground-penetrating radar) which has the advantages of being quick and nondestructive. However, it is difficult to capture reflection signals from small deep cavities with GPR (Sera et al., 2014). Mukunoki et al. (2005, 2009) found the wide spreading of low-density grounds above cavities with an X-ray CT scanner. Sato and Kuwano (2013); Kuwano et al. (2010) proposed the investigation of low-density grounds in order to develop new prevention measures. However, since no technique for sinkhole prevention has been fully established, it is necessary to clarify the causes of underground cavities and sinkholes in urban areas.

*Corresponding author.
E-mail addresses: msatolasperanza@gmail.com (M. Sato), kuwano@iis.u-tokyo.ac.jp (R. Kuwano).
Peer review under responsibility of The Japanese Geotechnical Society.

http://dx.doi.org/10.1016/j.sandf.2015.06.014

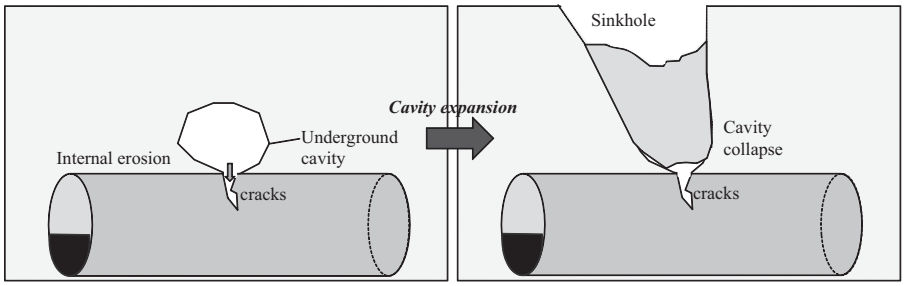

Fig. 1. Schematic figure of internal erosion from cracks in pipes.

Most studies on internal erosion focus on dams (e.g., Foster et al., 2000; Fell and Fry, 2007); pipes, which involve the preceding process of discharging soil to the cracks of sewer pipes. Researchers classify internal erosion by material properties, for example, concentrated leak erosion in core zones (e.g., Sherard et al., 1984a; Haghighi et al., 2013) and internal instability in filter zones (e.g., Sherard et al., 1984b; Wan and Fell, 2008; Moffat et al., 2011). Concentrated leak erosion is the enlargement of cracks in the core with high-pressurized water, while internal instability is a migration of the finer fraction through the coarser fraction with the seepage flow. Old artificial mines and sites with the chemical dissolution of rocks are mentioned as other places where the formation of underground cavities is induced. These issues are particularly threatening in areas such as Ohya, Japan, where there are old quarries (Yokoyama et al., 1997), and Florida, USA, where limestone layers are spread (Beck, 1988).

To our knowledge, there have been no recent studies on the influence of the seepage flow on the initiation of the internal erosion of subsurface structures. Underground structures are especially congested in urban areas, and sinkholes sometimes appear near these underground structures without the accompaniment of any obvious breakages. One hypothesis of this paper is the variation in the seepage direction, induced by the locations of subsurface structures, based on recent studies deeming that the seepage flow is significant to the progression of cavity expansion attributed to internal erosion. Sato and Kuwano (2010a); Tsutsumi et al. (2010) suggested that the hydraulic conductivity of materials affect the formation of cavities. In addition, Kuwano et al. (2012) investigated one sinkhole accident in Japan and found that it was caused by the erosion of highly permeable soil along the converged flow at the interface of the fills and the original ground. Kuwano et al. (2006) statistically investigated sinkhole accidents and discovered that they often occur in the rainy season.

The aim of this investigation was to reveal the mutual influence of underground structures on the development of underground cavities as a result of internal erosion, which is accompanied by a reduction in the strength of the ground. The contents of this paper are as follows. First, a series of laboratory model tests is described, simulating the progression of cavity expansion with the seepage flow in the ground including another subsurface structure. Second, an explanation of a series of laboratory penetration tests is given, and the penetration resistance of the model ground is measured after the model tests have been completed. Third, the methodology and the results of a large-scale model test are presented, and it is confirmed that the results of the above two series of laboratory experiments are applicable to practical grounds. In conclusion, a discussion is given on the process of the development of cavities and loose grounds with seepage localization.

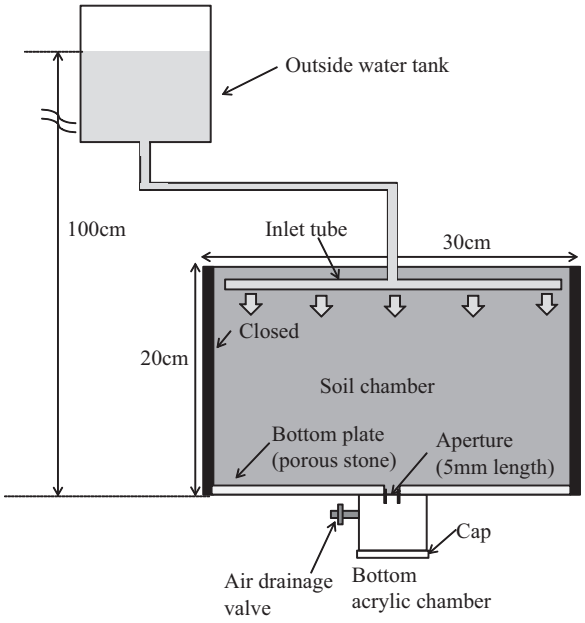

Fig. 2. Test apparatus used in laboratory model tests.

2. Laboratory model tests

2.1. Test apparatus and procedure

A new apparatus for laboratory testing was designed to perform experiments that allow soil discharge to the apertures by imposing on uniform seepage from the surface ground. Fig. 2 schematically shows the test apparatus which consists of a center soil chamber and a bottom acrylic chamber. The center soil chamber is 300 mm in length, 80 mm in thickness and 200 mm in height, including the aperture that is 5 mm in length and 80 mm in thickness at the center of the bottom of the soil chamber. The 1-g model test was applicable because a

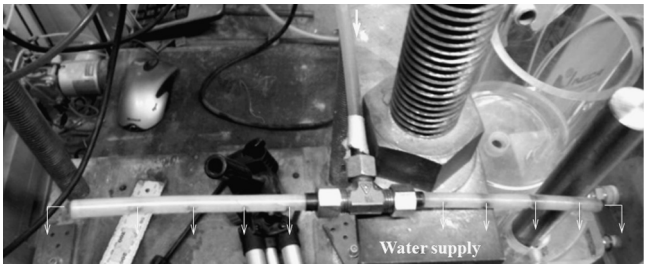

Photo 1. Inlet tube.

cavity was practically generated in the shallow ground (less than 2 m). In addition, the relationship between the grain size and the cracks of the model ground is similar to that of the field site. The front of the soil chamber is made of a transparent acrylic plate which allows for the visual observation of the ground. The hydraulic condition of the boundary of the apparatus is impervious at the side walls and permeable at the bottom. The base plates on the bottom of the soil chamber, as well as the model ground, are made of permeable porous stones. The bottom acrylic chamber is mounted to the bottom of the soil chamber and connected to the aperture for retrieving the discharged water and soil. An acrylic cylinder is used to simulate a subsurface pipe and is buried in the model ground for some test cases so that it is inflexible and fixed. The diameter and the thickness of the cylinder are 60 mm and 80 mm, respectively. The thickness of the soil chamber is equivalent to that of both the aperture and the cylinder; hence, the essentially identical deformation was considered along the thickness of the chamber.

We started our experiments by imposing a constant charge, 430 ml/min, from the inlet tube (Photo 1) connected to the outside water tank. The model ground was compacted by moist tamping into six layers including a thin portion of colored soil at the interface of each layer for the visible observation of the ground deformation. Tamping was done with a wooden stick until the fixed value for the thickness of each layer was achieved. Hime gravel ($G_s=2.65$, $D_{50}=1.7$ mm, $e_{max}=0.71$ and $e_{min}=0.48$) was subsequently placed on the surface of the model ground with a height of 20 mm. The inlet tube was buried in the Hime gravel layer to provide a uniform flow from the entire surface, which simulated water propagation from the surface due to rainfall. This pattern of water injection often occurs in shallow grounds. Other patterns have been inferred by Kuwano et al. (2010); Sato and Kuwano (2015). A great number of small holes were made in the surface of the inlet tube. This allowed for an adequately small and uniform flow of water from the water tank to prevent the disturbance of the gravel. The difference in head between the Hime gravel layer and the outside water tank was around 800 mm, and the charge was continued until the deformation reached the surface. It was difficult to perform an accurate operation on the total amount of inflow water because of the manual handling of both the onset and the termination of the water injection. Cavity formation and deformation were recorded by digital images from the front of the soil chamber until the end of both the soil and the water discharge from the aperture. The water content

Table 1
Test conditions.

Case	Material	Flow rate (ml/min)	Location of the cylinder	Onset of the soil discharge (s)
T_none	Toyoura	440	None	160
T_above	Toyoura	420	Above	140
T_far	Toyoura	440	Far	180
MixS_above	Mixed Silica	420	Above	220

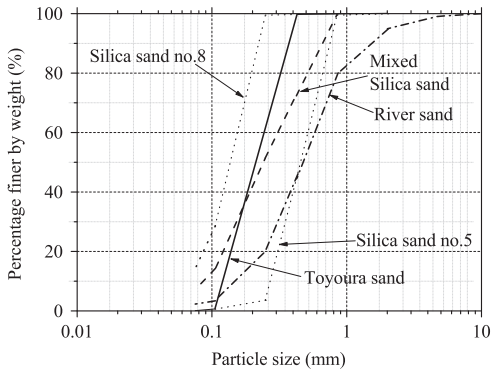

Fig. 3. Illustrated particle size distributions of materials.

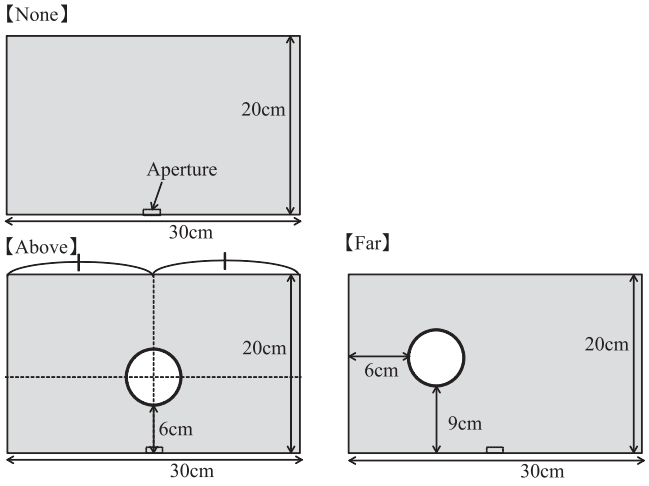

Fig. 4. Positions of cylinder.

of the model ground was measured at several points after the penetration test, and the dry mass of the discharged soil retrieved at the bottom acrylic chamber was also measured under a dry condition.

2.2. Test conditions

Table 1 lists the detailed testing conditions. The relative density and the initial water content were 80% and 10%, respectively, in all cases. The variables examined in the tests are the material and the location of the cylinder. Two kinds of materials were applied, namely, Toyoura sand ($G_s=2.62$, $e_{min}=0.64$ and $e_{max}=0.95$) and Mixed Silica sand for which

Silica sand no. 5 (G_s=2.64, e_{min}=0.56 and e_{max}=0.81) and Silica sand no. 8 (G_s=2.67, e_{min}=0.90 and e_{max}=1.51) were mixed under the weight ratio of 1:1. Toyoura sand was applicable to the laboratory model test, having been used in previous studies (e.g., Sato and Kuwano, 2010b, 2015). Mixed Silica sand was prepared in such a way that the material would have a similar average grain size to Toyoura sand without using clay fractions. If the testing material contained clay soil, it would take too long to generate cavities due to the low permeability. The test codes, for example, T_above, define the combination of tested material (Toyoura sand) and location of the cylinder (above). The particle size distributions of the testing materials are shown in Fig. 3.

As shown in Fig. 4, three locations are adopted for the cylinder, none, above and far. T_none is the test case; the cylinder is not placed in the ground. In the case of T_above, the cylinder is located just 60 mm above the aperture. Therefore, the distance from the aperture to the cylinder is nearer in the T_above case than in the T_far case. For the visual observation of the wetting front, colored ink is blended into the charging water in the cases of T_none and T_far. The location and the diameter of the cylinder in each case did not directly simulate specific actual situations. The aim of this research was to obtain the fundamental influence of the location of the cylinder by comparing each test case. The influence of structures with different shapes was described by Sato and Kuwano (2015). In addition, it should be pointed out that this research did not focus on the roughness of the surface cylinder, since the effect of the roughness was negligible. The rough surface caused a small increase in the deformation rate, but did not change the formation of the cavities, as described by Sato and Kuwano (2015).

2.3. Test results

2.3.1. No cylinder with Toyoura sand (test T_none)

Over a cumulative time of 160 s, from the start of the water charge (t=160 s), the onset of soil discharge was observed, followed by deformation right above the aperture, as shown in Photo 2(a). The development of a cavity following the deformation progressed straightly upward from the aperture to the opening, and a wetting front moved downward rapidly in the vicinity of the deformed portion and showed bilateral symmetry (t=180 s), as shown in Photo 2(b). The deformation finally induced a sinkhole at the ground surface, developed in a narrow area (the width was approximately 6 cm) from the aperture to the surface, as represented in Photo 2(c). The mass of the discharged soil was 998.71 g. The high water content above the aperture suggested the convergence of the seepage flow (Photo 2(c)).

2.3.2. Cylinder above aperture with Toyoura sand (test T_above)

Internal erosion commenced at time=140 s; and subsequently, the ground was deformed above the aperture, as shown in Photo 3(a). At time=200 s, the ground deformation

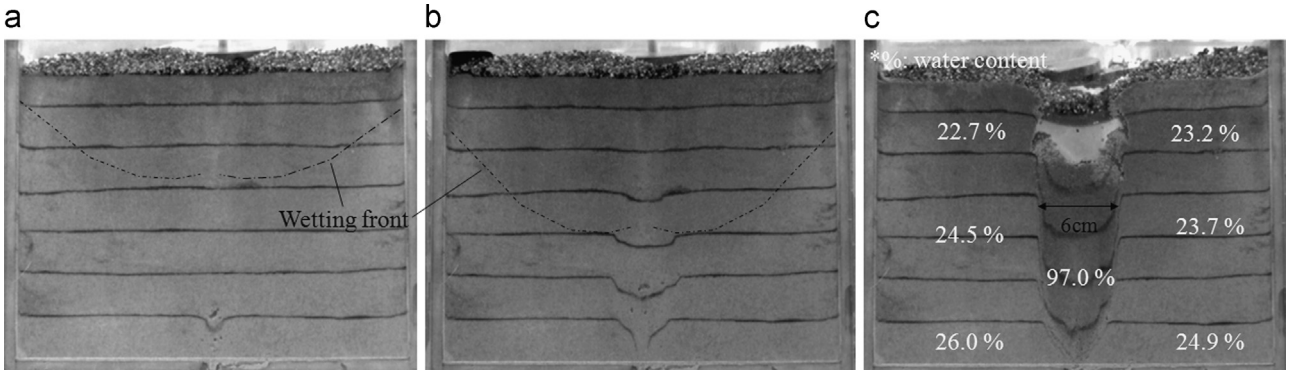

Photo 2. Progression of internal erosion, test T_none.

Photo 3. Progression of internal erosion, T_above.

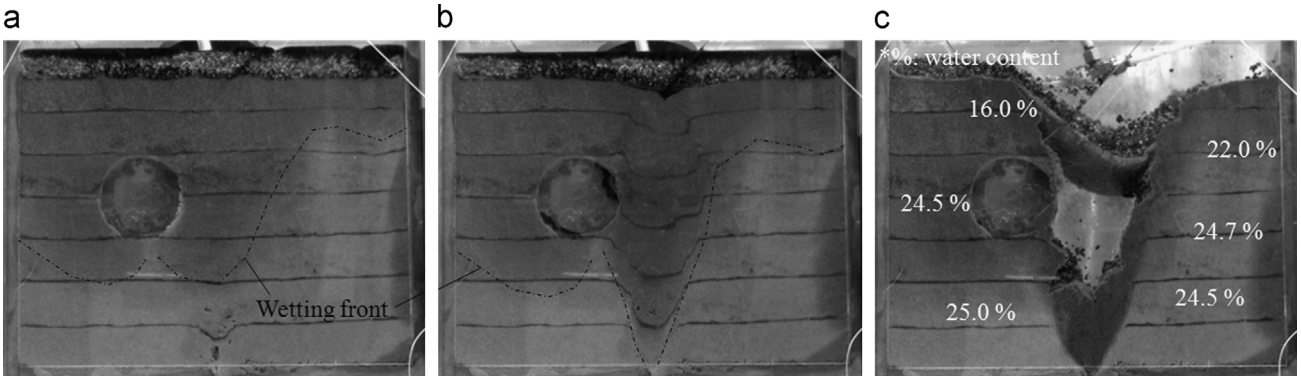

Photo 4. Visual observation of internal erosion, test T_far.

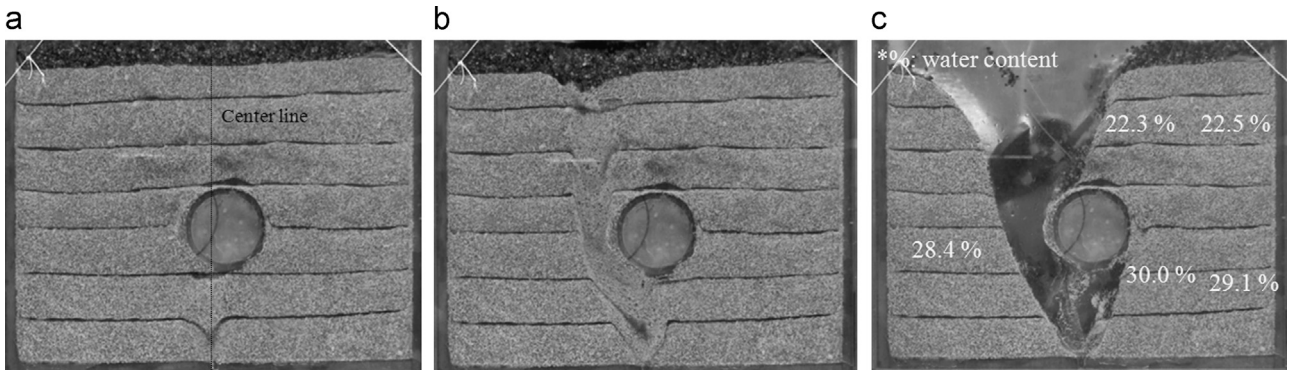

Photo 5. Visual observation of internal erosion, test MixS_above.

reached the surface through the left side of the cylinder (Photo 3(b)). The soil discharge continued until the cavity expanded throughout the preferential deformed portion to the left, and another deformed portion was encountered to the right, as shown in Photo 3(c). The difference between the right and the left was induced by the location of the cylinder, which was not placed accurately at the centerline along the height of the chamber, as demonstrated in Photo 3(a). The cylinder was a little to the right of the centerline of the ground and the distance from the surface to the aperture was smaller on the right. Therefore, the progression of internal erosion on the left occurred prior to that on the right. The water content was similar for the whole ground. It is supposed, therefore, that the water from the portion with the higher water content was mostly discharged and did not remain (Photo 3(c)). The mass of the eroded soil was 1683.78 g.

2.3.3. Cylinder far from aperture with Toyoura sand (test T_far)

The soil discharge to the aperture was initiated at $t=180$ s, similar to the preceding two cases. The wetting front migrated more rapidly to the right than to the left (Photo 4(a)). After the onset of erosion, deformation developed upward and a sinkhole occurred at time = 210 s, as shown in Photo 4(b). As a result of the erosion from the deformed portion, a cavity subsequently developed from the aperture to the surface (Photo 4(c)). The spatial progression of the cavity expansion on T_far was approximately similar to that on T_none. The water content was relatively uniform for the entire model ground (Photo 4(c)). The total mass of the discharged soil was 1693.74 g.

2.3.4. Cylinder above aperture with mixed silica sand (test MixS_above)

Photo 5(a)–(c) shows the visual observations on MixS_above. A comparison of T_above and MixS_above indicate that the spatial progression of MixS_above resembled that of T_above. The difference in the cavity formation between the right and the left sides of the ground was caused by a reason similar to that given for T_above, namely, the cylinder was located slightly to the right of the centerline (Photo 5(a)). In contrast, the temporal progression was slower in Mix_above than in T_above. Photo 5(c) illustrates that the lower portion had an approximately 5% higher water content than the upper portion, probably because of stagnation. The mass of the total drained loss was 1673.78 g.

3. Laboratory penetration tests

To evaluate the stiffness of the model ground, laboratory penetration tests were carried out following the laboratory model tests.

3.1. Test apparatus and procedure

A schematic figure of the device used for the laboratory penetration tests is shown in Fig. 5. The penetration resistance and the penetration depth were monitored by a load cell and an EDT (external displacement transducer), respectively, and recorded at 0.1 s intervals. A metal stick, 3 mm in diameter and 250 mm in length, was penetrated from the surface to a height of approximately 50 mm from the bottom of the chamber with a constant rotation of 100 rpm (around 0.15 mm/s). All the measured points were located 40 mm from the front and the back of the model chamber, in other words, on the centerline along the thickness (80 mm) of the chamber. The locations of the points in each test series are described with the test results.

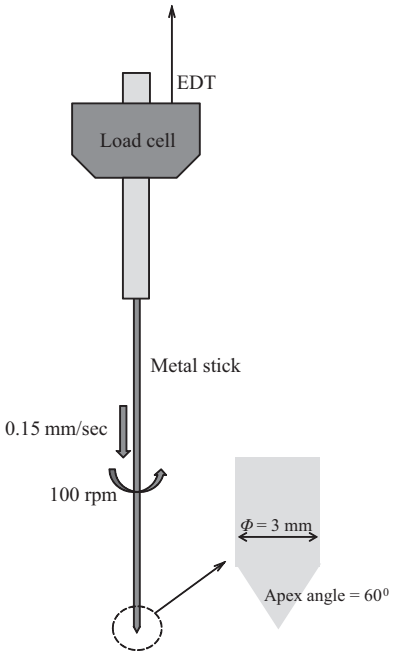

Fig. 5. Test apparatus for penetration tests.

3.2. Test results

Photo 6 illustrates the measured lines of penetration resistance along the height of the model ground. In this paper, the disturbed portion is defined as the enclosed portion in which penetration

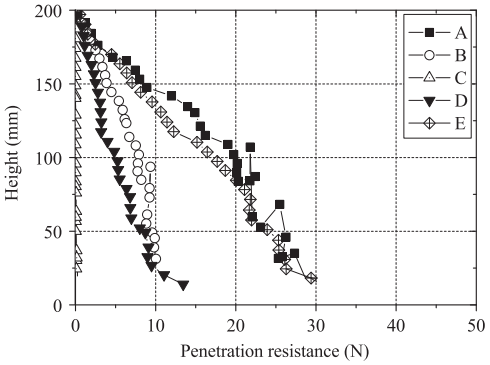

Fig. 6. Penetration resistance of T_none.

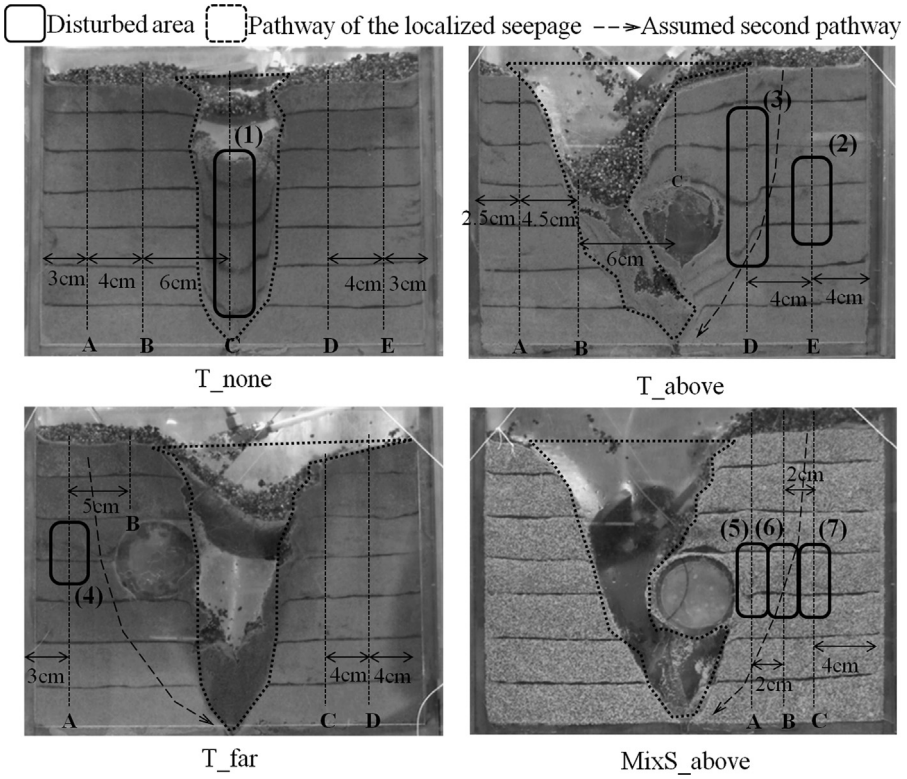

Photo 6. Concentrated seepage area and disturbed area in each test case.

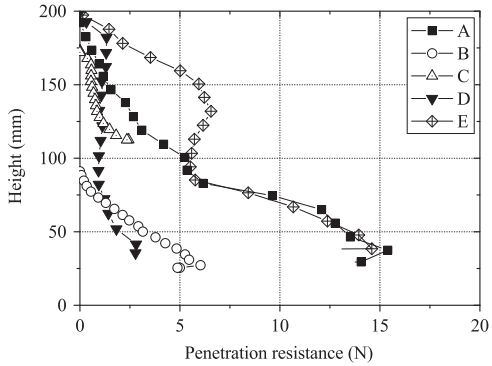

Fig. 7. Penetration resistance of T_above.

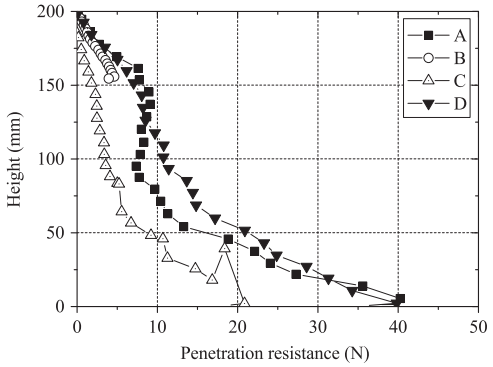

Fig. 8. Penetration resistance of T_far.

resistance was not increased along each measured line accompanying the progress of the penetration of the metal stick. Previous studies, using a similar apparatus, reported that the resistance was monotonously increased for the rise in penetration depth due to the increase in the confining pressure when the ground was not disturbed (e.g., Renuka and Kuwano, 2011; Sera et al., 2014).

3.2.1. No cylinder with Toyoura sand (test T_none)

Fig. 6 shows the change in penetration resistance with the change in height for the T_none case. Deformed portion C hardly showed any resistance and contained small cavities inside the ground. Other parts were symmetrical at the centerline in the perpendicular direction of the soil chamber; the nearer to the wall, the larger the resistance.

3.2.2. Cylinder above aperture with Toyoura sand (test T_above)

Deformed portion D had the lowest penetration resistance, although the value was not exactly zero due to the remaining soil. The penetration resistance of the other portions decreased in proportion to the distance from the side walls, except for lines A and B. The resistance of A was smaller than that of B due to the cavity near line A (Fig. 7 and Photo 6).

3.2.3. Cylinder far from aperture with Toyoura sand

Fig. 8 represents the results of the penetration tests for the T_far case. No significant disturbed area could be confirmed, and the effect of the distance from the chamber walls was identified similarly to the other test cases mentioned above.

3.2.4. Cylinder above aperture with mixed silica sand (test MixS_above)

Only the right-side ground was measured in the MixS_above case, since the length of the left-side ground was not adequate for the penetration of the stick as a result of the cavity formation. A comparison of MixS_above and T_above showed that the trend in the disturbed portion in the former was different from that in the latter, although both the spatial progression of the cavity expansion and the position of the cylinder were essentially identical in the two cases (see Figs. 7 and 9). The penetration resistance of all three lines was decreased in a similar location, ranging in height from 75 mm to 125 mm. The height of the disturbed portion

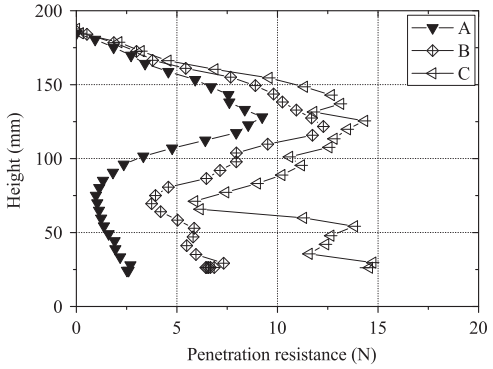

Fig. 9. Penetration resistance of MixS_above.

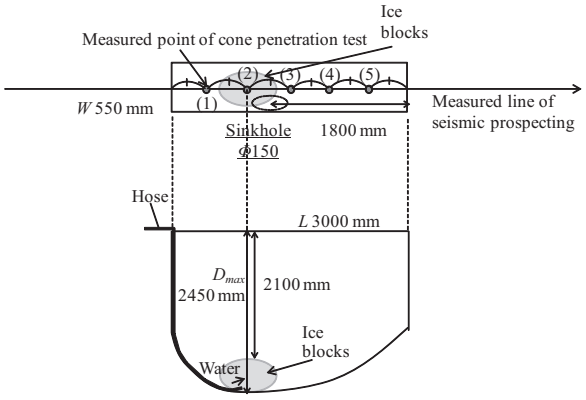

Fig. 10. Schematic figure of large-scale model test.

approximately corresponded to that of the cylinder. The penetration resistance was inversely proportional to the distance from the walls, similar to the other cases.

4. Large-scale model test

4.1. Test apparatus and procedure

Fig. 10 shows a schematic figure of the large-scale model test, applied to a pit 3000 mm in length, 2450 mm maximum in depth and 550 mm in thickness. The cavity was artificially created at the bottom of the ground by the melting of ice blocks. Four ice blocks were initially placed right below point

(2) and connected to a vinyl hose. The size of each ice block was roughly 300 mm × 400 mm × 200 mm, and the surface of the ice blocks was located at a depth of 2100 mm. These parameters were approximately equivalent to the actual scale of the sinkhole accidents; therefore, the test results were applicable to the field sites. After the ice blocks were placed, river sand, with a relative density of approximately 80%, was used as backfilling under neither too dense nor too loose conditions. Fig. 3 shows the particle size distribution of river sand as being a highly permeable and widely graded sandy material. Subsequently, water was supplied through the hose for about one and a half hours in order to melt the ice blocks. Following the stoppage of the water supply, the ground in the pit was matured for several hours. The penetration resistance was measured at five points by means of a portable cone penetration test (JGS 1431) and the seismic prospecting was inspected at the centerline on the surface along the length of the pit before and after the supply of water.

4.2. Test results

An hour after the initiation of the supply of water, a small sinkhole, approximately 150 mm in diameter, appeared at the surface (Photo 7). Fig. 11 shows the penetration resistance acquired at the five points in the ground after the ground was matured for several hours. As for the ground above the ice blocks, the overall ground under point (2) and the ground near the bottom under point (1) had very low penetration resistance. This suggests that the disturbed portion above the cavity had developed widely due to the melting of the ice blocks. The pulse velocity distribution in the ground was estimated from the results of the seismic prospecting (Fig. 12). The velocity was reduced for the overall ground of the pit after pouring the water, and the maximum reduction ratio was 50% compared with the ground before the pouring of the water, which showed that the ground was loosened and disturbed.

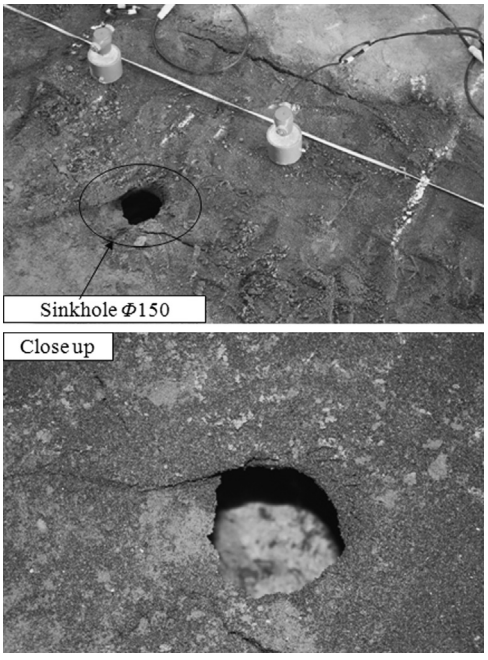

Photo 7. Sinkhole at surface of ground.

5. Discussion

5.1. Factor of cavity expansion

The combination of two factors for the spatial and temporal progression of cavity expansion, as a result of internal erosion, has been proposed in this paper. One factor was the pathway of localized seepage and the other factor was the hydraulic conductivity of the ground. The spatial progression of the cavity expansion was governed by the pathway of the localized seepage from the surface to the aperture and the fact that the location of the cylinder yields a variation in the pathway generated through the nearest path from the surface to the aperture. The sudden onset of soil discharge from the aperture occurred due to the saturation of the entire pathway; and consequently, a cavity developed rapidly along the liquefied pathway, following the transient deformation. Liquefaction was implied from the decrease in penetration resistance in the specified area, which corresponded to the loss of effective stress. Liquefaction, induced by excess pore water pressure, was also suspected because the hydraulic gradient in the model ground exceeded the theoretical critical one under saturated conditions. The hydraulic gradient ($i=\Delta h/L$) of the model ground achieved a value of approximately 4.0, since the difference in head (Δh) was approximately 800 mm and the minimum length of the seepage path (L), equivalent to the nearest distance from the surface to the aperture, was approximately 200 mm. This value was not exact because the ground was not completely saturated, although the ground close to the aperture was supposed to be almost saturated. On the other hand, the critical hydraulic gradient (represented by $(G_s-1)/(1+e)$) was deduced as 0.95 for the Toyoura sand in the model ground ($G_s=2.62$, $e_{80}=0.70$), and the value was assumed to be similar for the Mixed Silica sand. After the cavity was connected from the surface to the aperture, the seepage converged through the second nearest path. Localized seepage was also indicated due to the very high water content in the deformed portion in the T_none case (Photo 2). A comparison of T_above and MixS_above suggests that the material properties were not significant factors in the spatial progression of the cavity expansion.

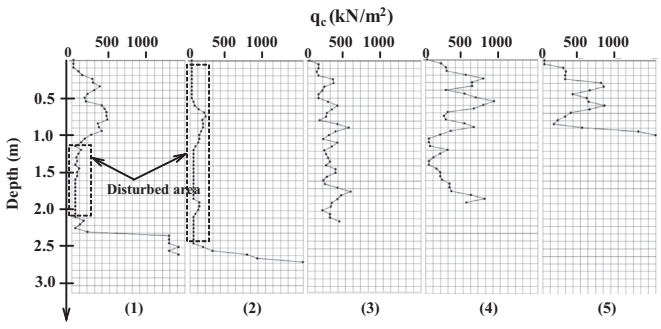

Fig. 11. Penetration resistance of large-scale model test.

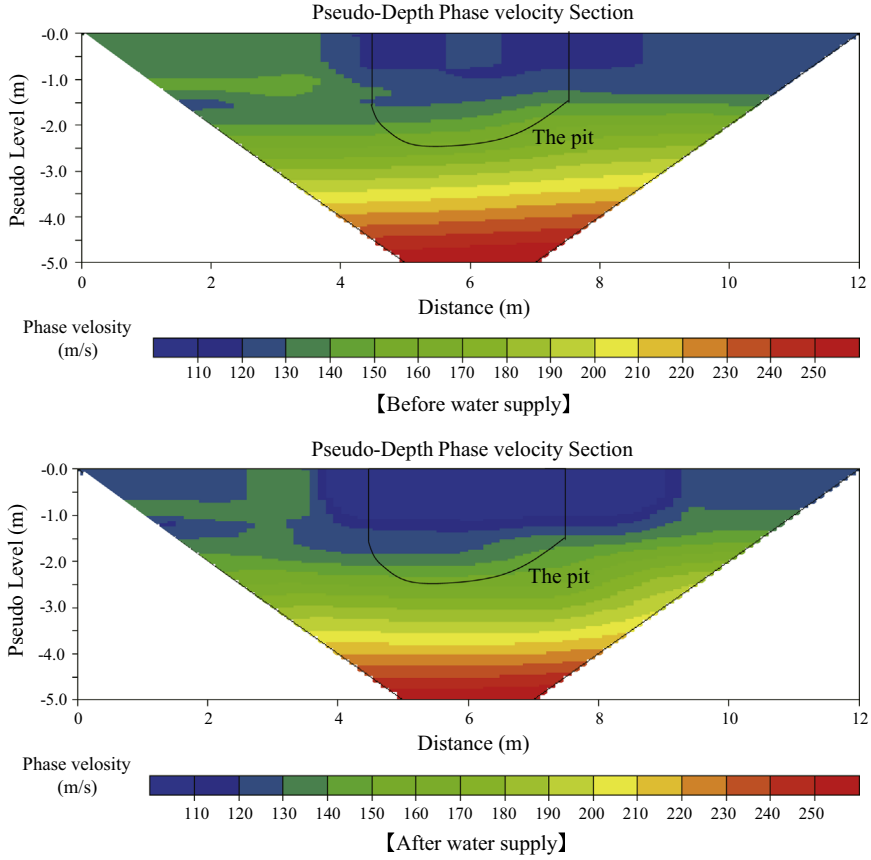

Fig. 12. Seismic prospecting before and after water supply.

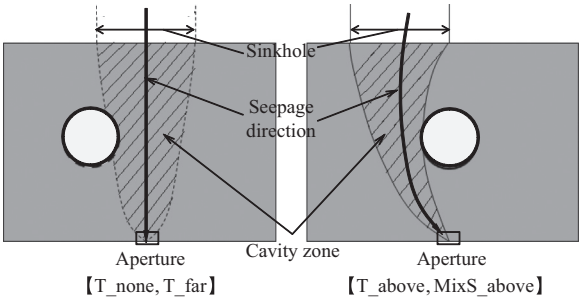

Fig. 13. Two different types of cavity and sinkhole formations.

Based on the preceding hypothesis, the types of spatial progression of the cavity and the disturbed portion are separated into two groups: (1) T_none and T_far and (2) T_above and MixS_above. A schematic figure of these two types is illustrated in Fig. 13. A comparison of group (1) and group (2) indicates that both the cavity and the sinkhole formation were varied by the cylinder located right above the aperture. In contrast, the similarity between T_none and T_far indicates that the cylinder far from the original pathway of the localized seepage did not substantially influence the formation of the cavity.

The temporal progression of the cavity expansion was governed by the hydraulic conductivity associated with both the pathway of the localized seepage and the material properties. The onset time of the soil discharge from the aperture is shown in Table 1. By comparing the test series of Toyoura sand cases, it is seen that erosion was induced most rapidly in T_above, for which the cylinder was in the original pathway of the localized seepage, owing to the high hydraulic conductivity at the interface of the cylinder and the ground, according to Sato and Kuwano (2010b, 2015). High hydraulic conductivity at the subtle gap of the cylinder was also implied by the rapid movement of the wetting line on the left, including the cylinder, in the case of T_far (Photo 4(c)) Hydraulic conductivity was mostly yielded by the material properties; hence, the temporal progression was slower for the Mixed Silica sand containing fine particles. Incidentally, the tested materials in this paper were non-cohesive soil and did not contain any clayey fractions. Cohesive soil is presumed to have disparate behavior because of low permeability (Horii et al., 2005).

5.2. Pathway of localized seepage

The pathway of the localized seepage is defined as the portion from the aperture to the ground where the cavity and the deformation primarily occurred, as represented in Photo 6. The area was estimated from the digital images taken from the front of the soil chamber at the end of the model tests. To obtain the derivation of the eroded soil, the amount of soil which was equivalent to the mass of the soil in the pathway

was calculated by Eq. (1).

$$S_c = \rho_d \times W \times A_c \quad (1)$$

S_c is the amount of soil in the pathway (g); ρ_d is the density of the material in a dry condition (g/cm^3); ρ_d is the density of the material in a dry condition (g/cm^3); W is the width of the soil chamber (cm); A_c is the area of the pathway of localized seepage (cm^2).

If S_c was similar to the amount of discharged soil, it means that almost all the soil was eroded through the pathway of localized seepage. In this test series, the parameters are given as $W=8$ cm and $\rho_d=1.553$ g/cm^3 for Toyoura sand and 1.491 g/cm^3 for Mixed Silica sand. The deformation was approximately similar along the direction of width and regarded as a two-dimensional deformation. Consequently, $W=8$ cm was estimated. The mass of the discharged soil, A_c and S_c for each test case, are listed in Table 2. A_c was based on the visible deformation induced by the seepage force; it was not related to the zonation of the water propagation. Furthermore, S_c was approximately similar to the amount of discharged soil in all test cases, except for T_none, which verified the hypothesis that only the water-saturated soil along the pathway was involved in the internal erosion and the soil discharge from the aperture, as mentioned in Section 5.1. It was noted in the T_none case that the soil remained in the pathway, depending on the early stoppage of the water charge; consequently, S_c exceeded the mass of the drained soil. Until the cavity expansion reached the surface ground and had completely grown from the surface to the aperture, the amount of discharged soil was linearly proportional to the water injection volume, as described by Sato and Kuwano (2010a).

5.3. Disturbed portion

The locations of the disturbed portions are summarized in Photo 6. The deformed portions, such as portions (1) and (3), had remarkably low resistance, attributed to the increase in void ratio. In deformed portion (3), the ascent of the void ratio is examined by the change in thickness of each colored sand layer along the height of the chamber, as shown in Photo 8. The equation is given as

$$\Delta e = \left(\frac{L_n'}{L_n} - 1\right) \times 100 \quad (2)$$

L_n is the initial thickness of the nth layer from the top; L_n' is the thickness of the nth layer at the end of the test; Δe is the rise in void ratio (%).

Table 2
Mass of discharged soil, A_c and S_c.

Case	Total discharged soil (g)	A_c (cm^2)	S_e (g)
T_none	998.71	108	1341
T_above	1683.78	121	1503
T_far	1693.74	127	1578
MixS_above	1673.78	135	1677

The layers not inducing soil drainage were calculated from the first to third layers. The increase in void ratio with the approach to the aperture inferred that the disturbed portion grew upward with soil drainage from the aperture (Table 3), as well as the growth of the cavity and deformation. The trends of the estimated void ratio corresponded to the penetration resistance, which increased in the first layer, and subsequently decreased in the second and third layers. The upward progression of the disturbed portion in the laboratory model ground was in accordance with the trend indicated in the large-scale model test.

Portions (2), (4), (5), (6) and (7) were disturbed without the accompaniment of visible deformation. Portions (5), (6) and (7) were continuous along the horizontal direction, with the same ranges for each line in the vertical direction. These portions were located in the vicinity of the second concentrated seepage path, where the invisible migration of the soil particles would preferentially occur. In addition, the portions were spread near the cylinder, where the seepage effluent converged owing to a reduction in the cross-sectional area. Meanwhile, internal instability was not induced, according to Kenny's H-F standard (Kenny and Lau, 1985). Both Toyoura sand and Mixed Silica sand were regarded as stable materials not containing any mobile finer particles. It is proved that no apparent change occurred in the particle size distribution of either the drained or the original grading distribution, as illustrated in Fig. 14.

The penetration resistance was susceptible to the distance from the walls of the soil chamber. In general, a change in the penetration resistance is inversely correlated to a change in the disturbance from the walls, as mentioned above. Fig. 15 illustrates the plots of the penetration resistance at heights of 150 mm and 100 mm versus the distance from the side walls for the three cases of Toyoura sand. The lower portion of the ground was affected by the bottom wall; hence, this study is only focused on the upper portion of the ground. In all test cases, penetration resistance was decreased by increasing the distance from the walls. A comparison of the three cases shows that T_none had the largest penetration

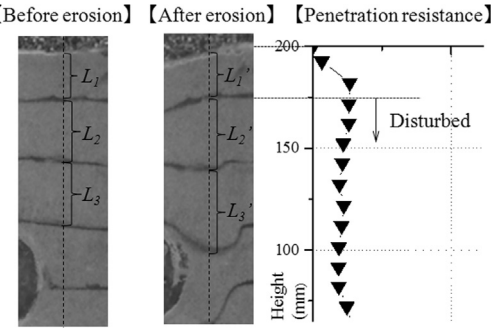

Photo 8. Rise in void ratio of T_above.

Table 3
Calculated void ratio in each layer.

Nth layer	Δe (%)
1	0
2	5
3	30

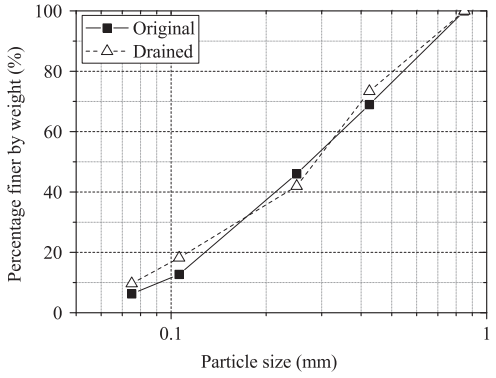

Fig. 14. Particle size distribution of drained soil in MixS_above.

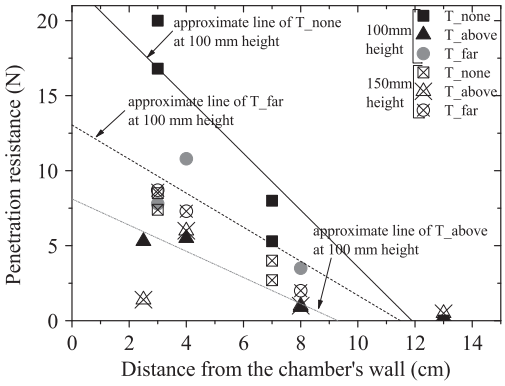

Fig. 15. Relationship between penetration resistance and distance from side walls.

resistance, which may have been caused by the smallest amount of discharged soil in the T_none case. The resistance of T_above was lower than that of T_far, despite the fact that the amount of drained soil was approximately equivalent in both cases. It was inferred that the disturbed area was widely developed in the T_above case because of the variation in the pathway of the localized seepage.

5.4. Development process of cavities and disturbed portion as a result of internal erosion

The above-mentioned discussions are summarized for the process of the development of underground cavities and disturbed portions as a result of internal erosion in the case of the ground including subsurface structures.

1) Seepage flow is localized throughout the nearest path from the surface to the outlet.
2) The saturation near the outlet induces the eruption of soil discharge to it.
3) A cavity develops following transient deformation along the entire liquefied pathway.
4) The cavity expands from the outlet to the surface.
5) Seepage is localized through the second nearest path.
6) (2)–(5) are repeated

Fig. 16 shows a schematic figure of the preceding process. The descent of the penetration resistance implies that the effective stress had widely diminished in the ground prior to the visible deformation. In the large scale model test, the process was stopped at the transient deformation in process (3), for the soil discharge was limited to the volume of the ice block.

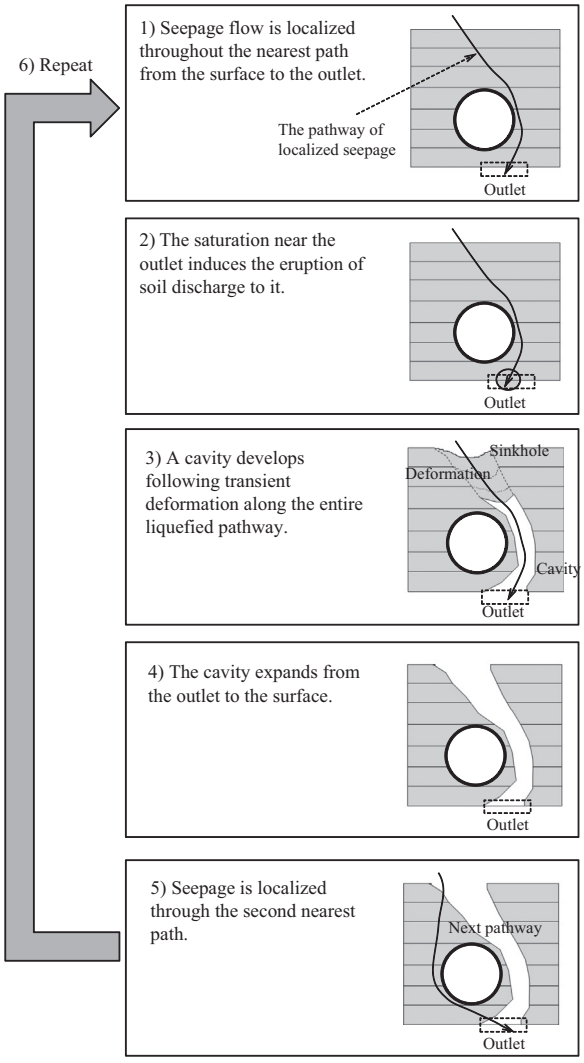

Fig. 16. Process of generation of underground cavities with internal erosion.

6. Conclusions

It has been revealed in earlier studies that localized seepage and hydraulic conductivity affect the water penetration in the ground. Meanwhile, the novel contribution of this research was to obtain the mutual influence of underground structures on sinkhole accidents and seepage localization, and to examine the penetration resistance for an evaluation of the strength of the ground being imposed by internal erosion. A program of various laboratory experiments was conducted using the developed laboratory apparatus and a practical scale ground. The conclusions of this study are described below.

i. Cavity growth, accompanied by internal erosion, occurred preferentially throughout the pathway of the localized seepage to the aperture. The localization was very

susceptible to the distance from the aperture, induced along the nearest path from the surface to it. The cylinder brought about a variation in the pathway when it was located near the original pathway. Following the episodic onset of erosion from the outlet, a cavity developed along the pathway due to the internal erosion of the liquefied soil.

ii. The spatial progression of the cavity expansion was governed by seepage localization, as described above. On the other hand, the temporal progression of the cavity expansion was governed by the hydraulic conductivity which was yielded by both the location of the cylinder and the material properties.

iii. A change in the penetration resistance correlated with a change in the distance from the cavities, and inversely from the walls of the soil chamber. A remarkable descent in the resistance was induced in the deformed portion. Furthermore, the disturbed ground spread extensively without being accompanied by visible deformation, which also occurred in a practical scale of the ground.

iv. In practical situations, seepage localization can be predicted from spatial relationships between the outlet and other structures, and causes a variation in the locations of sinkhole accidents at the surface ground. Therefore, it is significant to consider not only the broken pipes, but also the sound ones.

Acknowledgments

This research was financially supported by Tokyo Gas Co., Ltd., Grant-in-Aid for JSPS Fellows (no. 11J08637) and Grant-in-Aid for Scientific Research (B, no. 19360210). The large-scale model test was carried out at the Public Works Research Institute (PWRI). The seismic prospecting data were collected with the aid of a practitioner at Chuo-Kaihatsu, while the cone penetration test of the large-scale model test was conducted with the help of members at Geo-Search Co., Ltd.

References

Beck, B., 1988. Environmental and engineering effects of sinkholes—the processes behind the problems. Environ. Geol. Water Sci. 12 (2), 71–78.

Erosion of Geomaterials. In: Bonelli, S. (Ed.), ISTE Ltd. and John & Sons, Inc..

Internal Erosion of Dams and Their Foundations. In: Fell, R., Fry, J.J. (Eds.), Taylor & Francis.

Foster, M., Fell, R., Spannagle, M., 2000. The statistics of embankment dam failures and accidents. Can. Geotech. J. 37, 1000–1024.

Haghighi, I., Chevalier, C., Duc, M., Guédon, S., 2013. Improvement of hole erosion test and results on reference soils. J. Geotech. Geoenviron. Eng. 139 (2), 330–339.

Horii, T., Kuwano, R., Kohashi, H., Katano, S., 2005. Model test on process of cavity generation above old underground pipe. In: Proceedings of 40th Japan National Conference of Geotechnical Engineering, Hakodate, pp. 1919–1920. (in Japanese).

Kenny, T.C., Lau, D., 1985. Internal stability of granular filters. Can. Geotech. J. 22, 215–225.

Kuwano, R., Horii, T., Kohashi, H., Yamauchi, K., 2006. Defects of sewer pipes causing cave-ins in the road. In: Proceedings of Fifth International Symposium on New Technologies for Urban Safety of Mega Cities in Asia, Phuket, pp. 347–353.

Kuwano, R., Sera, R., Sato, M., 2010. Formation of subsurface cavity and loosening due to defected old sewer pipe. Jpn. Geotech. J. 5 (2), 219–229.

Kuwano, R., Kohata, Y., Sato, M., 2012. Case study of ground cave-in due to subsurface erosion in old landfill. In: Proceedings of Sixth International Conference on Scour and Erosion, Paris, pp. 56–62.

Moffat, R., Fannin, R.J., Garner, S.J., 2011. Spatial and temporal progression of internal erosion in cohesionless soil. Can. Geotech. J. 48, 399–412.

Mukunoki, T., Otani, J., Nonaka, S., Horii, T., Kuwano, R., 2005. Evaluation of cavity generation in soils subjected to sewerage defects using X-ray CT. In: Proceedings of Second International Workshop on X-Ray CT for Geomaterials, Grenoble & Aussois, pp. 365–371.

Mukunoki, T., Kumano, N., Otani, J., Kuwano, R., 2009. Visualization of three-dimensional failure in sand due to water inflow and soil drainage from defected underground pipe using X-ray CT. Soils Found. 49 (6), 959–968.

Renuka, S., Kuwano, R., 2011. Formation and evaluation of loosened ground above a cavity by laboratory model test with uniform sand. In: Proceedings of 13th International Summer Symposium of JSCE, Uji, pp. 211–214.

Sato, M., Kuwano, R., 2010a. Model tests for the evaluation of formation and expansion of a cavity in the ground. In: Proceedings of Seventh International Conference on Physical Modelling in Geotechnics, Zurich, pp. 581–586.

Sato, M., Kuwano, R., 2010b. Fundamental study of permeability change around buried structures in sandy ground. In: Proceedings Eighth International Symposium on New Technologies for Urban Safety of Mega Cities in Asia, Kobe, pp. 607–615.

Sato, M., Kuwano, R., 2013. Effects of buried structures on the form of underground cavity. In: Proceedings of 18th International Conference on Soil Mechanics and Geotechnical Engineering, pp. 1769–1772.

Sato, M, Kuwano, R., 2015. Influence of buried structures on underground seepage and generation of cavities. Jpn. Geotech. J. 10 (1), 113–125 (publishing, in Japanese).

Sera, R., Koike, Y., Kuwano, R., Kuwano, J., 2014. Sub-surface cavities in the liquefied ground caused by the Great East Japan Earthquake. Jpn. Geotech. J. 9 (3), 323–339.

Sherard, J.L., Dunnigan, L.P., Talbot, J.R., 1984a. Filters for silts and clays. J. Geotech. Eng. 110 (6), 701–718.

Sherard, J.L., Dunnigan, L.P., Talbot, J.R., 1984b. Basic properties of sand and gravel filters. J. Geotech. Eng. 110 (6), 684–700.

Tohda, J., Yoshimura, H., 2001. A new design method for buried pipelines subjected to differential ground settlement. In: Proceedings of 15th International Conference on Soil Mechanics and Geotechnical Engineering, pp. 1319–1322.

Tohda, J., Hachiya, M., 2005. Response and design of buried pipelines subjected to differential ground settlement. In: Proceedings of 16th International Conference on Soil Mechanics and Geotechnical Engineering, pp. 1659–1662.

Tsutsumi, Y., Kuwano, R., Sato, M., 2010. Local deformation characteristics of model ground with cavity and loosening. In: Proceedings of Seventh International Conference on Physical Modelling in Geotechnics, Zurich, pp. 587–592.

Wan, C.F., Fell, R., 2008. Assessing the potential of internal instability and suffusion in embankment dams and their foundations. J. Geotech. Geoenviron. Eng. 134 (3), 401–407.

Yokoyama, Y., Imaizumi, K., Ueno, K., Mizunuma, T., 1997. Study on the mechanism of subsidence into the underground cavity in Ohya quarries. J. Jpn. Soc. Civ. Eng. 568 (iii-39), 113–123.